SDF2 promotes glioma progression via GRP78-mediated ERAD and copper homeostasis disruption

AOXIANG LI[1], XIAOLONG LI[2], TUO WANG[3] and JINNING SONG[3]

[1]Department of Neurosurgery, Xi'an International Medical Center Hospital, Xi'an, Shaanxi 710300, P.R. China;
[2]Department of Interventional Radiology, Affiliated Hospital of Yan'an University, Yan'an, Shaanxi 716000, P.R. China;
[3]Department of Neurosurgery, First Affiliated Hospital of Xi'an Jiaotong University, Xi'an, Shaanxi 710061, P.R. China

Received March 10, 2025; Accepted June 19, 2025

DOI: 10.3892/ijmm.2025.5595

Abstract. Stromal cell-derived factor 2 (SDF2) is an endoplasmic reticulum chaperone protein crucial for protein folding. Its role in gliomas is poorly understood. The present study investigated SDF2 expression and function in glioma progression. Our data revealed that the expression of SDF2 was upregulated in glioma tissues. In glioma cell lines, SDF2 promoted cell proliferation and migration, whereas the knockdown of SDF2 (Ad-shSDF2) induced cell death. Further investigations revealed that the copper chelator tetrathiomolybdate (TTM) could reverse the reduction in cell viability caused by Ad-shSDF2. Upon SDF2 knockdown, the expression of ATP7A and ATP7B was decreased in glioma cells, whereas the expression of glucose-regulated protein 78 (GRP78) was increased. Moreover, the proteasome inhibitor MG132 and the silencing of GRP78 effectively blocked the Ad-shSDF2-mediated decrease in ATP7A and ATP7B expression, as well as the accumulation of dihydrolipoamide S-acetyltransferase in mitochondria. *In vivo*, SDF2 promoted subcutaneous tumor growth in nude mice, an effect that could be reversed by overexpression of GRP78. This reversal was accompanied by an increase in the intra-tumoral copper ion concentration. In gliomas, SDF2 promotes tumor growth by inhibiting the GRP78-mediated endoplasmic reticulum-associated degradation pathway, thereby increasing the expression of ATP7A and ATP7B. This results in reduced intracellular accumulation of copper ions, facilitating tumor progression.

Correspondence to: Dr Tuo Wang or Dr Jinning Song, Department of Neurosurgery, First Affiliated Hospital of Xi'an Jiaotong University, 277 Xiguan Street, Beilin, Xi'an, Shaanxi 710061, P.R. China
E-mail: tuowang_xjd@163.com
E-mail: jinningsong@126.com

Key words: glioma, stromal cell-derived factor 2, glucose-regulated protein 78, endoplasmic reticulum-associated degradation, cuproptosis

Introduction

Glioma, the most common malignant tumor of the central nervous system, poses a significant challenge in the field of neuro-oncology due to its high invasiveness and poor response to conventional treatments (1). Despite advancements in surgical interventions, radiotherapy and pharmacotherapy, the prognosis of glioma remains unfavorable, with a short survival period (2). In recent years, researchers have explored targeted therapies and immunotherapies in hopes of improving treatment outcomes and survival rates for these patients (3). However, despite progress in existing treatment modalities, the high recurrence rate and therapeutic resistance of gliomas significantly complicate their clinical management (4). Hence, investigating these molecular mechanisms not only aids in elucidating the biological characteristics of gliomas but also provides a theoretical basis for the development of new targeted therapeutic strategies.

The endoplasmic reticulum (ER) is a continuous network of membrane-bound tubular structures within the cytoplasm that is primarily responsible for the folding, modification, transport and degradation of proteins (5). ER-associated degradation (ERAD) is a highly conserved quality control mechanism that plays a crucial role in identifying and disposing of misfolded proteins by retro-translocating them into the cytoplasm for proteasomal degradation (6). This process involves several key steps, including substrate recognition, extraction, polyubiquitination, and subsequent degradation via ERAD, in which molecular chaperones and lectins recognize unfolded or misfolded nascent polypeptides (7). These misfolded proteins bind to chaperones and are then delivered to ERAD ligands (7,8). Ultimately, the polyubiquitinated substrates are translocated through the retro-translocation channel into the cytoplasm, where they are degraded by the 26S proteasome (8,9). Glucose-regulated protein 78 (GRP78, Bip), a prominent ER chaperone, not only assists in protein folding but also plays a pivotal role in the ERAD pathway by recognizing misfolded proteins and facilitating their retro-translocation, highlighting its importance in maintaining ER homeostasis and cellular health (Fig. 1) (10). Cuproptosis is a recently identified form of programmed cell death characterized by the accumulation of copper ions, which bind to lipoylated proteins in the mitochondrial tricarboxylic acid cycle (Fig. 2). This

interaction leads to protein aggregation, loss of iron-sulfur cluster proteins, proteotoxic stress, and ultimately, cell death. Emerging evidence indicates a significant interplay between cuproptosis and ER stress pathways (11,12). In cervical cancer, the curcuminoid analog PBPD (1-propyl-3,5-bis(2-bromobenzylidene)-4-piperidinone) has been shown to induce cuproptosis by modulating the Notch1/RBP-J/NRF2/FDX1 signaling axis (11). Specifically, PBPD suppresses Notch1 and RBP-J expression, leading to decreased NRF2 activity and subsequent upregulation of FDX1. This cascade results in increased oxidative stress, activation of ER stress responses, and induction of cuproptosis in cervical cancer cells. In lung adenocarcinoma, it has been demonstrated that copper accumulation activates the unfolded protein response (UPR), particularly through the spliced form of X-box binding protein 1 (XBP1s) (12). Hence, targeting the molecular crosstalk between ER stress and copper-induced cell death pathways may offer novel therapeutic strategies for cancers characterized by disrupted copper homeostasis and ER stress responses.

Stromal cell-derived factor 2 (SDF2) acts as an ER chaperone protein, primarily facilitating protein folding, enhancing chaperone activity, maintaining ER functionality, and regulating stress responses (13). SDF2 forms a complex with ER DnaJ heat shock protein 3 (ERdj3), helping to maintain the folded state of newly synthesized proteins and preventing misfolding and aggregation (14). Its presence enhances the chaperone activity of ERdj3, making it more effective at inhibiting protein aggregation under normal physiological conditions. By associating with ERdj3 and SDF2-like protein 1, SDF2 contributes to the maintenance of ER quality control mechanisms, ensuring the proper function of intracellular proteins (14). Under ER stress conditions, the role of SDF2 may be linked to the secretion of ERdj3 and its extracellular functions, aiding cells in addressing the challenges of protein folding (15). Therefore, the primary function of SDF2 in the ER is to serve as a molecular chaperone that promotes and maintains the correct folding of proteins, thereby ensuring normal physiological activities and stress responses in cells (Fig. 1) (15). However, its role in glioma remains unexplored. The objective of the present study was to investigate the specific functions and mechanisms of SDF2 in glioma development and progression.

Materials and methods

Cell culture. The glial cell lines U87 (cat. no. CL-0238), U251 (cat. no. CL-0237) and HMC3 (cat. no. CL-0620; all from Procell Life Science & Technology Co., Ltd.) were cultured in complete MEM (HyClone; Cytiva) supplemented with 10% fetal bovine serum (FBS), 1% non-essential amino acids, sodium pyruvate and penicillin-streptomycin. The cells were maintained in a humidified incubator at 37˚C with 5% CO_2. When the cells reached ~85% confluence, they were passaged using trypsinization. All cell lines were authenticated using STR profiling.

MG132 treatment. To investigate the involvement of the proteasome degradation pathway in the downregulation of ATP7A and ATP7B, U87 and U251 glioma cells were treated with the proteasome inhibitor MG132. Specifically, cells were incubated with MG132 (cat. no. HY-13259; MedChemExpress) at a final concentration of 10 μM for 24 h.

Western blotting. Protein extraction was performed from cells or tissue samples using RIPA lysis buffer (Beijing Solarbio Science & Technology Co., Ltd.). The lysates were centrifuged at 10,000 x g for 15 min to remove cellular debris, and the supernatant containing the total protein was collected. Protein concentrations were quantified using a BCA assay. Equal amounts of protein samples (15 μg/lane) were then subjected to 10% SDS-PAGE. Following electrophoresis, the proteins were transferred onto a PVDF membrane (MilliporeSigma). The membrane was then blocked with 5% non-fat milk or BSA (cat. no. A8010; Beijing Solarbio Science & Technology Co., Ltd.) in TBST (TBS with 0.1% Tween-20) for 1 h at room temperature. The membrane was incubated overnight at 4˚C with primary antibodies specific to the target proteins SDF2 (cat. no. PK47764), SDF2L1 (cat. no. PK17377), ERdj3 (cat. no. PA2683), GRP78 (cat. no. T55166), ATP7A (cat. no. PA7106), ATP7B (cat. no. TA0410), dihydrolipoamide S-acetyltransferase (DLAT; cat. no. T58125) and GAPDH (cat. no. M20006; 1:1,000; all purchased from Abmart Pharmaceutical Technology Co., Ltd.). Lipoic acid (cat. no. 437695) was purchased from MilliporeSigma. After washing with TBST to remove unbound primary antibodies, the membrane was incubated with HRP-conjugated secondary antibodies (cat. no. ZB-2301 for rabbit; cat. no. ZB-2305 for mouse) Beijing Solarbio Science & Technology Co., Ltd.) for 1 h at room temperature. Following several washes with TBST, the bound antibodies were visualized using an enhanced chemiluminescence (ECL) detection system (Beijing Solarbio Science & Technology Co., Ltd.). The intensity of each protein band was quantified using ImageJ analysis software (version 10; Media Cybernetics, Inc.). GAPDH was used as an internal control.

Reverse transcription-quantitative PCR (RT-qPCR). Total RNA was extracted from cells using TRIzol reagent, and cDNA was synthesized following the instructions provided with the PrimeScript™ RT Master Mix (Perfect Real Time) (Takara Bio, Inc.). The reverse transcription conditions were set at 37˚C for 15 min, followed by 85˚C for 5 sec and then 4˚C indefinitely. For qPCR, a 20-μl reaction mixture consisting of 10 μl of Applied Biosystems™ SYBR Green Master Mix (Thermo Fisher Scientific, Inc.), 1 μl each of forward and reverse primers, 2 μl of cDNA, and 6 μl of ddH_2O was prepared. The PCR protocol included initial denaturation at 95˚C for 30 sec, followed by 40 cycles of amplification with denaturation at 95˚C for 5 sec, annealing at 60˚C for 30 sec, and extension at 72˚C for 30 sec. qPCR was conducted on a LightCycler 480 system (Roche Diagnostics) to quantify gene expression. The primers used in the present study were listed as follows: SDF2 forward, 5'-GGAGCTTGGCATCATGGACT-3' and reverse, 5'-GGAGCTTCATAGCGTCTCCA-3'; CHOP forward, 5'-ATGAACGGCTCAAGCAGGAA-3' and reverse, 5'-GGGAAAGGTGGGTAGTGTGG; GRP78 forward, 5'-TCAGGCCAAGCCCAATACAG-3' and reverse, 5'-TCCACGGTAGTGAGAGCCTT-3'; XBP1s forward, 5'-TGCTGAGTCCGCAGCAGGTG-3' and reverse, 5'-GCTGGCAGGCTCTGGGGAAG-3'; XBP1u forward, 5'-ACGGGACCCCTAAAGTTCTG-3' and reverse,

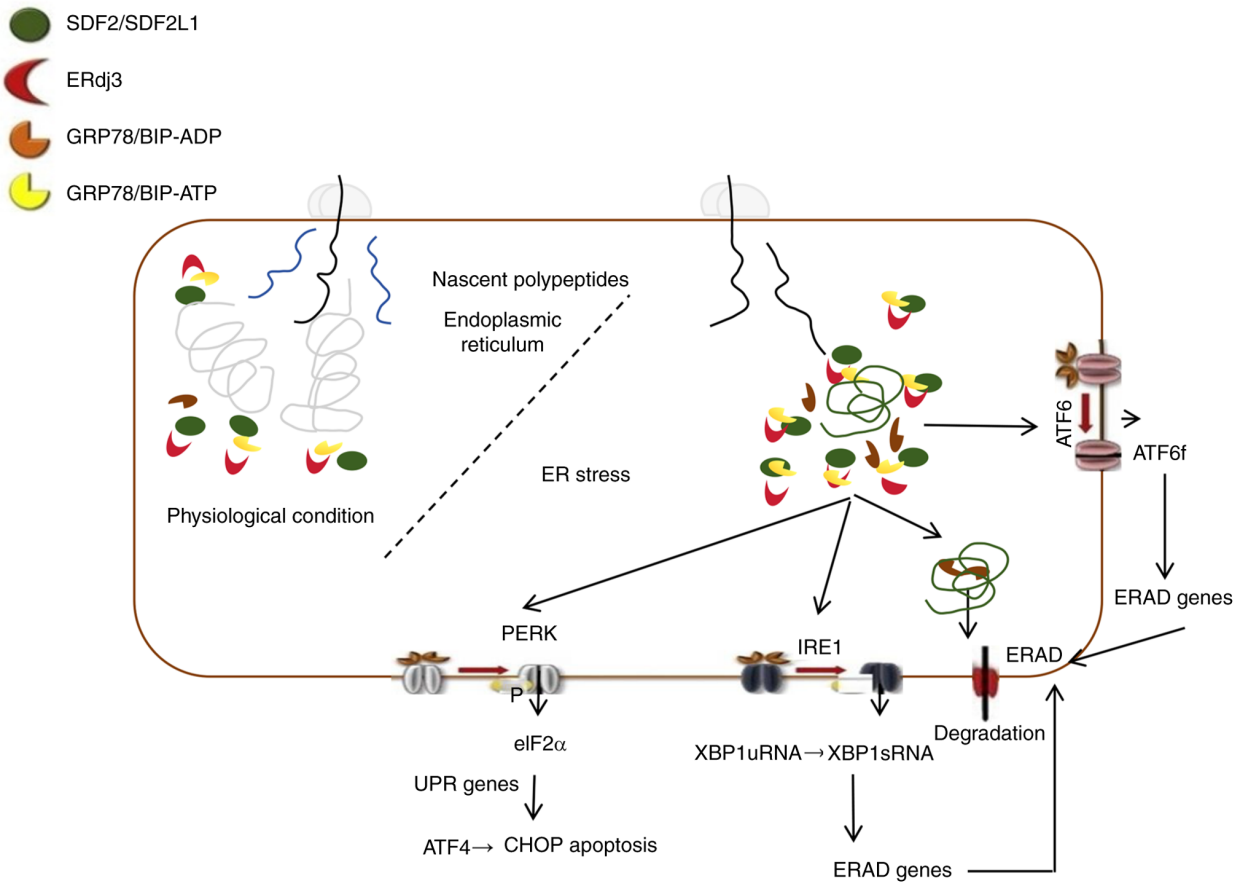

Figure 1. Schematic molecular mechanism of SDF2 in ER stress. SDF2, stromal cell-derived factor 2; ER, endoplasmic reticulum; ERAD, ER-associated degradation; GRP78, glucose-related protein 78; UPR, unfolded protein response; XBP1, X-box binding protein 1; ERdj3, endoplasmic reticulum DnaJ heat shock protein 3.

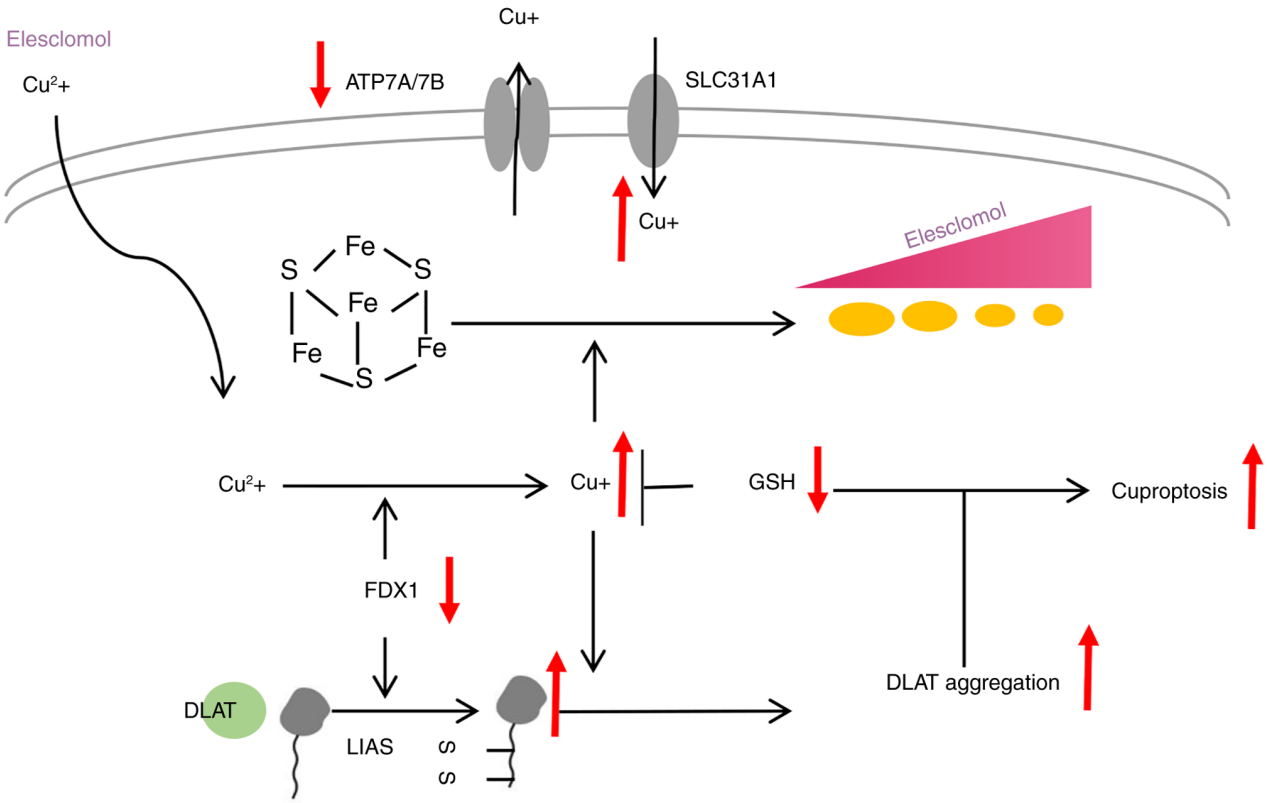

Figure 2. Schematic molecular mechanism of cuproptosis. GSH, reduced glutathione.

5'-TGCACGTAGTCTGAGTGCTG-3'; and GAPDH forward, 5'-CCAGCAAGAGCACAAGAGGA-3' and reverse, 5'-GGG GAGATTCAGTGTGGTGG-3'. The $2^{-\Delta\Delta Cq}$ method was used for quantification assay (16).

Human samples. Human tumor and adjacent non-tumor tissue samples were obtained from patients with glioma during surgical procedures, with informed consent obtained from all participants. A total of 10 patients were enrolled in the present study, including 4 females and 6 males. The median age was 66 years (range, 53-67 years). Ethical approval for sample collection and study was granted by the institutional review board of the First Affiliated Hospital of Xi'an Jiaotong University (approval no. 2024SF-FAHX-212; Xi'an, China).

Additionally, the GEPIA database (http://gepia.cancer-pku.cn/) was used to analyze SDF2 mRNA expression levels across various tissue types and pathological conditions. Statistical significance was assessed using GEPIA's integrated analytical tools, providing insights into the potential role of SDF2 in disease pathology.

Detection of malondialdehyde (MDA), reduced glutathione (GSH) and adenosine triphosphate (ATP). Cells from each group were collected, and the levels of MDA, reduced GSH and ATP were measured using the appropriate assay kits in strict accordance with the manufacturers' protocols. The lipid peroxidation level was assessed using an MDA Assay kit (cat. no. S0131S), ATP levels were quantified using an ATP Assay kit (cat. no. S0026), and GSH and oxidized glutathione (GSSG) levels were measured using a GSH and GSSG Assay kit (cat. no. S0053) (all from Beyotime Institute of Biotechnology).

EdU (5-Ethynyl-2'-deoxyuridine) detection. The procedure was conducted using a BeyoClick EdU Cell Proliferation Kit (DAB method) (cat. no. C0085S; Beyotime Institute of Biotechnology). Briefly, cells were incubated in medium containing 10 μM EdU for 2 h. After EdU labeling, the medium was removed, and 1 ml of 4% paraformaldehyde (PFA; cat. no. P0099; Beyotime Institute of Biotechnology) was added to each well before incubation at room temperature for 15 min. The fixative was then removed, and the cells were washed three times with 1 ml of wash solution per well, with each wash lasting 5 min. Following the wash steps, 1 ml of PBS containing 0.3% Triton X-100 was added to each well, and the cells were incubated at room temperature for 15 min to permeabilize the cells. Next, 0.5 ml of Click reaction solution was added to each well, and the cells were incubated in the dark at room temperature for 30 min. The Click reaction solution was then aspirated, and the cells were washed three times with wash solution, with each wash lasting 5 min. Finally, the cells were mounted with antifade mounting medium containing DAPI (a final concentration of 1 μg/ml) and observed under a fluorescence microscope.

Transwell assay. The bottom membrane of the Transwell insert (Corning, Inc.) was coated with Matrigel matrix (Corning, Inc.) at 37˚C for 1 h. U87 and U251 glioma cells, which were cultured to ~85% confluence, were harvested using trypsinization and centrifuged at 1,000 x g for 15 min. The cell density was adjusted to $5x10^3$ cells/100 μl, and the cells were resuspended in serum-free medium to create a single-cell suspension. Transwell inserts (8 μm pore size) were placed in a 24-well plate, 600 μl of serum-containing medium was added to the lower chamber to act as a chemoattractant, and 200 μl of the treated cell suspension was added to the upper chamber. After 24 h of incubation, the inserts were removed, and the remaining medium was aspirated. The inserts were washed with PBS and fixed with 4% PFA for 30 min at room temperature, followed by staining with 0.1% crystal violet for 15 min. The cells that had migrated through the membrane were visualized and images were captured under an inverted light microscope (Keyence Corporation). The number of invasive cells was quantified using ImageJ software.

Flow cytometric analysis of apoptosis using Annexin V-PE/7-AAD staining. Cells in the logarithmic growth phase were harvested by trypsinization, collected in centrifuge tubes, and resuspended in PBS. After the cells were counted, $5x10^5$ cells were collected and washed with PBS. The cells were then resuspended in binding buffer from an Annexin V-PE/7-AAD Apoptosis Detection Kit (cat. no. E-CK-A216; Elabscience Biotechnology, Inc.) and incubated in the dark at room temperature for 20 min. Following incubation, the cells were washed, resuspended and analyzed for apoptosis by flow cytometry (CytoFLEX; Beckman Coulter, Inc.). The data were analyzed using FlowJo 10 (FlowJo LLC). The experiment was performed in triplicate for statistical reliability.

Quantification of intracellular reactive oxygen species (ROS) levels by flow cytometry. Intracellular ROS levels were measured by flow cytometry using a fluorescent probe-based ROS detection kit (Wuhan Servicebio Technology Co., Ltd.). Briefly, the cells were washed twice with PBS, centrifuged at 800 x g for 5 min to remove the supernatant at room temperature, and collected. DCFH-DA working solution was then added to each sample at a density of $1x10^5$ cells/ml, and the cells were incubated at 37˚C in a CO_2 incubator protected from light for 30 min. After incubation, the cells were centrifuged at 800 x g for 5 min to remove the DCFH-DA solution, followed by washing with PBS 3 times to ensure the removal of excess probe. The cells were finally resuspended in PBS and immediately analyzed by flow cytometry for ROS detection.

siRNA transfection. For transfection, cells were seeded in 6-well plates at a density of $4x10^5$ cells per well 24 h prior to transfection to achieve optimal confluency. Small interfering RNA (siRNA, 5'-AAAUAGAACAUUUUGAAGGUG-3') targeting the gene of interest and a non-targeting control siRNA (NC, 5'-UUCUCCGAACGUGUCACGUTT-3') were obtained from Shanghai GenePharma Co., Ltd. Transfection was performed using HiPerFect Transfection Reagent (cat. no. 301705; Qiagen, Inc.) following the manufacturer's protocol. Briefly, 150 ng of siRNA (final concentration of 10 nM) was diluted in 100 μl of serum-free DMEM. Subsequently, 6 μl of HiPerFect Transfection Reagent was added to the diluted siRNA solution, mixed gently, and incubated at room temperature for 10 min to allow complex formation. The siRNA-lipid complexes were then added dropwise to each well containing cells in

2 ml of complete growth medium. Cells were assessed 48 h post-transfection.

Cell Counting Kit-8 (CCK-8) assay. U87 and U251 cells were adjusted to a density of 1,000 cells/μl and seeded into a 96-well plate. The cells were incubated at 37˚C in a 5% CO_2 incubator for 24 h. After incubation, the medium was removed, and the wells were washed with PBS. Fresh medium (100 μl) was added to each well, followed by 10 μl of CCK-8 solution (Beijing Solarbio Science & Technology Co., Ltd.). The plate was then incubated for an additional 1 h. Absorbance was measured at 450 nm using a microplate reader to assess cell viability. The experiments included the following groups: Ad-NC and Ad-shSDF2. To investigate the mechanisms underlying the reduction in cell viability induced by Ad-shSDF2, several inhibitors were added to the Ad-shSDF2 group: z-VAD (20 μM), Nec-1 (10 μM), VX-765 (10 μM), Fer-1 (1 μM), and TTM (10 μM). Cell viability was calculated based on absorbance (A450) values, allowing for the assessment of each inhibitor's effect on Ad-shSDF2-induced cell viability reduction and identification of the specific cell death pathways involved.

Detection of copper ion content. The intracellular copper ion content was quantified using a Copper (Cu^{2+}) Colorimetric Assay kit (Elabscience Biotechnology, Inc.). For the assay, 15 μl of each of the eight copper standards at different concentrations, as well as 15 μl of each test sample, were added to individual wells. Then, 230 μl of chromogenic working solution was added to each well. The plates were covered with sealing film and incubated at 37˚C for 5 min. The optical density (OD) of each well was measured at 580 nm using a microplate reader.

Detection of intracellular copper ions. The intracellular copper ion distribution was visualized using the fluorescent probe Coppersensor 1 (MedChemExpress). Cells were incubated with the probe at a final concentration of 5 μM in each well, protected from light, at 37˚C for 30 min. After incubation, the cells were observed under a fluorescence microscope to assess the localization and intensity of copper ion fluorescence.

Detection of mitochondrial ROS. Mitochondrial ROS levels were detected using the specific fluorescent probe MitoTracker Red CMXRos (Beyotime Institute of Biotechnology). Once the cells reached the desired density, the culture medium was removed and replaced with MitoTracker Red CMXRos working solution at a final concentration of 1 μM. The cells were incubated at 37˚C for 30 min. After incubation, the working solution was removed, and prewarmed fresh culture medium was added. Fluorescence was observed using a fluorescence microscope to assess the mitochondrial ROS levels.

Immunofluorescence (IF). U87 and U251 cells were seeded in six-well plates at a density of $5x10^5$ cells per well and incubated at 37˚C with 5% CO_2 until adherence. After 24 h, the cells were fixed with 500 μl of 4% PFA for 30 min, followed by permeabilization with 500 μl of 0.1% Triton X-100 for 30 min. The cells were then blocked with IF blocking buffer for 1 h. After the blocking solution was removed, a mixture of primary antibodies against TOM20 and DLAT (Abcam) was added (50 μl per well), and the cells were incubated overnight at 4˚C. The next day, the primary antibodies were removed, and the cells were incubated with the appropriate secondary antibodies (500 μl per well) at room temperature, protected from light, for 1 h. DAPI staining solution (a final concentration of 1 μg/ml) was then applied for 5 min to stain the nuclei. Images were captured and stored using an inverted fluorescence microscope.

Co-immunoprecipitation (co-IP). For these experiments, a co-IP kit (cat. no. P0401; GENESEED; https://www.geneseed.com.cn/web/lxwm.html) was used. Briefly, protein extracts were prepared using RIPA lysis buffer (Beijing Solarbio Science & Technology Co., Ltd.). A specific antibody against GRP78 was added to the protein samples to allow binding with the target protein, and the samples were incubated at 4˚C for several hours or overnight. 30 μl of protein A or G magnetic beads (50% concentration) were then added to bind the antibody-protein complexes, which were collected using magnetic separation. The beads were washed multiple times with lysis buffer to remove non-specifically bound proteins. The immunoprecipitated proteins were then eluted from the beads by heating or by adding an elution buffer. Finally, the eluted proteins were separated by SDS-PAGE and analyzed by western blotting to detect co-immunoprecipitated proteins. By normalizing the Co-IP results to GAPDH levels, any potential discrepancies in protein loading were accounted for and it was ensured that the observed decrease in ATP7A and ATP7B co-precipitation was specifically attributable to the reduced availability of GRP78 for interaction, rather than other experimental variations.

Construction of adenoviral vectors. Adenoviral vectors were constructed by Vigene Biosciences for the overexpression and knockdown of the SDF2 or GRP78 proteins. Adenoviral vectors carrying negative control genes (Ad-NC, UUCUCC GAACGUGUCACGUTT) or shRNA sequences (Ad-sh-SDF2, UCUUUUUGCCCACUGAUAGGU) targeting SDF2 were designed to infect cells. Adenoviral vectors were added at a concentration of 10^9 PFU/ml, with 20 μl viral suspension per well in six-well plates. After incubation at 37˚C for 24 h, the viral-containing medium was removed, cells were washed with PBS, and fresh medium was added.

Xenograft tumor model in mice. A total of 15 SPF-grade BALB/c nude male mice (6-8 weeks old, 18-22 g, Cyagen Biosciences; https://www.lascn.net/SupplyDemand/Site/Index.aspx?id=30) were randomly assigned into three experimental groups (Ad-NC, Ad-SDF2, and Ad-SDF2 + Ad-GRP78), with five mice per group, using a computer-generated randomization schedule. This sample size was selected based on precedent studies and accepted practices in glioma xenograft models, where comparable group sizes have been sufficient to detect statistically significant effects (17-19). Investigators responsible for data collection and outcome assessment were blinded to group allocation to minimize potential bias. All animals were acclimatized to the laboratory environment for one week prior to experimentation and housed under standard specific pathogen-free (SPF) conditions [22±2˚C, 55±10% humidity, 12/12-h light/dark cycle

(7:00-19:00), with *ad libitum* access to diet and sterile water]. Logarithmically growing U251 cells were collected from each treatment group. Cell pellets were resuspended in 200 μl of ice-cold PBS to maintain viability and kept on ice until injection. Each mouse was subcutaneously injected with $1x10^6$ cells into the inguinal region. Tumor implantation was designated as day 0. Tumor growth and general health were monitored every two days. Tumor volume (mm^3) was measured using calipers and calculated according to the formula: volume=1/2 x longest diameter (mm) x [shortest diameter (mm)]^2. At the experimental endpoint, mice were euthanized by cervical dislocation. Subcutaneous tumors were excised, weighed, and processed for further analysis. The maximum tumor diameter observed was 8.2 mm, corresponding to a volume of 106.64 mm^3. All animal procedures were approved by the Institutional Animal Care and Use Committee of the Animal Experimentation Center, Xi'an Jiaotong University (approval no. XJTUAE2023-1944; Xi'an, China).

Immunohistochemistry (IHC). Tumor tissue sections were subjected to Ki-67 IHC. In brief, the tissues (5 μm) were deparaffinized in xylene, rehydrated in a graded ethanol series, and treated with 3% hydrogen peroxide to inactivate endogenous peroxidase activity. Antigen retrieval was performed, followed by blocking with goat serum (cat. no. C0625; Beyotime Institute of Biotechnology). Ki-67 primary antibody (1:200; cat. no. AB2008; Beyotime Institute of Biotechnology) was applied, and the samples were incubated overnight at 4˚C. The sections were then incubated with HRP-conjugated goat anti-rabbit IgG (cat. no. A0208; Beyotime Institute of Biotechnology) at 37˚C for 30 min, followed by the application of DAB substrate for color development (30 sec). Hematoxylin counterstaining was performed for 1 min, and differentiation was achieved in 1% hydrochloric acid ethanol. The sections were then dehydrated through a graded ethanol series, cleared in xylene, and mounted with neutral resin. Images were captured using a light microscope. In each field, the number of Ki-67-positive tumor cell nuclei and the total number of tumor cell nuclei were manually counted. The proliferation index was then calculated as the percentage of Ki-67-positive cells among the total tumor cells in each field, and the average of these five fields was taken as the final proliferation index for the sample.

Statistical analysis. Statistical analyses were performed using GraphPad Prism software (version 10.0; Dotmatics). The data are presented as the mean ± standard deviations (SDs). For relative expression graphs, the control group was normalized to a fixed value (for example, 1 or 100%). For comparisons between two groups, an unpaired two-tailed Student's t-test was employed. For comparisons among multiple groups, one-way analysis of variance was conducted, followed by Tukey's post hoc test to assess pairwise differences between group means. $P<0.05$ was considered to indicate a statistically significant difference.

Results

Increased expression of SDF2 in glioma tissues. Bioinformatic predictions revealed an increase in SDF2 mRNA expression in glioma tissues compared with control tissues (Fig. 3A and B). Consistently, RT-qPCR analysis revealed significantly elevated SDF2 mRNA levels in tumor tissues relative to adjacent normal tissues (Fig. 3C). IF staining further demonstrated an increase in SDF2 fluorescence intensity in glioma tissues compared with control tissues (Fig. 3D). Western blot analysis confirmed higher SDF2 protein expression in glioma samples than in adjacent non-tumor tissues (Fig. 3E). These findings collectively suggest that SDF2 expression is upregulated in glioma, potentially implicating it in glioma pathogenesis.

SDF2 promotes malignant proliferation in glioma cells. U87 and U251 cells were transfected with Ad-SDF2 to overexpress SDF2. Following SDF2 overexpression, both the mRNA and protein levels of SDF2 were significantly elevated in U87, U251 and HMC3 cells (Fig. 4A-F). Additionally, cell viability assays demonstrated that, compared with the control, SDF2 overexpression enhanced the viability of U87 and U251 cells in a time-dependent manner (Fig. 4G and H), but the viability of HMC3 cells did not change (Fig. 4I). The EdU staining results further confirmed that SDF2 overexpression increased the proliferative capacity of U87 and U251 cells relative to that of the controls (Fig. 4J-M). Moreover, Transwell assays indicated that SDF2 overexpression promoted the migratory ability of U87 and U251 cells (Fig. 4N and O). These findings suggest that SDF2 plays a role in promoting the malignant proliferation and migration of glioma cells.

Knockdown of SDF2 increases ROS levels and cuproptosis in glioma cells. U87 and U251 cells were transfected with Ad-shSDF2 to achieve SDF2 knockdown. The mRNA and protein levels were decreased in U87 and U251 cells transfected with Ad-shSDF2 (Fig. 5A-D). Compared with the control, Ad-shSDF2 transfection resulted in a significant increase in the proportion of late apoptotic and necrotic cells in both the U87 and U251 lines (Fig. 5E and F). Additionally, ROS levels were significantly elevated following SDF2 knockdown in U87 and U251 cells, indicating increased oxidative stress (Fig. 5G and H). Interestingly, only the cuproptosis inhibitor TTM reversed the decrease in viability induced by Ad-shSDF2 in U87 and U251 cells (Fig. 5I and J). These results suggest that SDF2 knockdown induces oxidative stress, increases apoptosis, and may involve copper-dependent cell death pathways in glioma cells.

Knockdown of SDF2 induces copper ion accumulation in glioma cells. In both the U87 and U251 cell lines, SDF2 knockdown led to a significant increase in the intracellular copper ion concentration compared with that in the controls. This finding was confirmed through fluorescence staining (Fig. 6A) and further quantified using colorimetric assays (Fig. 6B and C). Additionally, the expression of the copper-exporting proteins ATP7A and ATP7B, as well as FDX and lipid-DLAT, was reduced in U87 and U251 cells following SDF2 knockdown, whereas DLAT protein levels remained unchanged (Fig. 6D and E). Furthermore, SDF2 knockdown resulted in decreased intracellular GSH levels (Fig. 6F) and increased ROS and MDA levels, indicating elevated oxidative stress and lipid peroxidation within the cells (Fig. 6G and H). These results suggest that SDF2 plays a role in maintaining copper homeostasis,

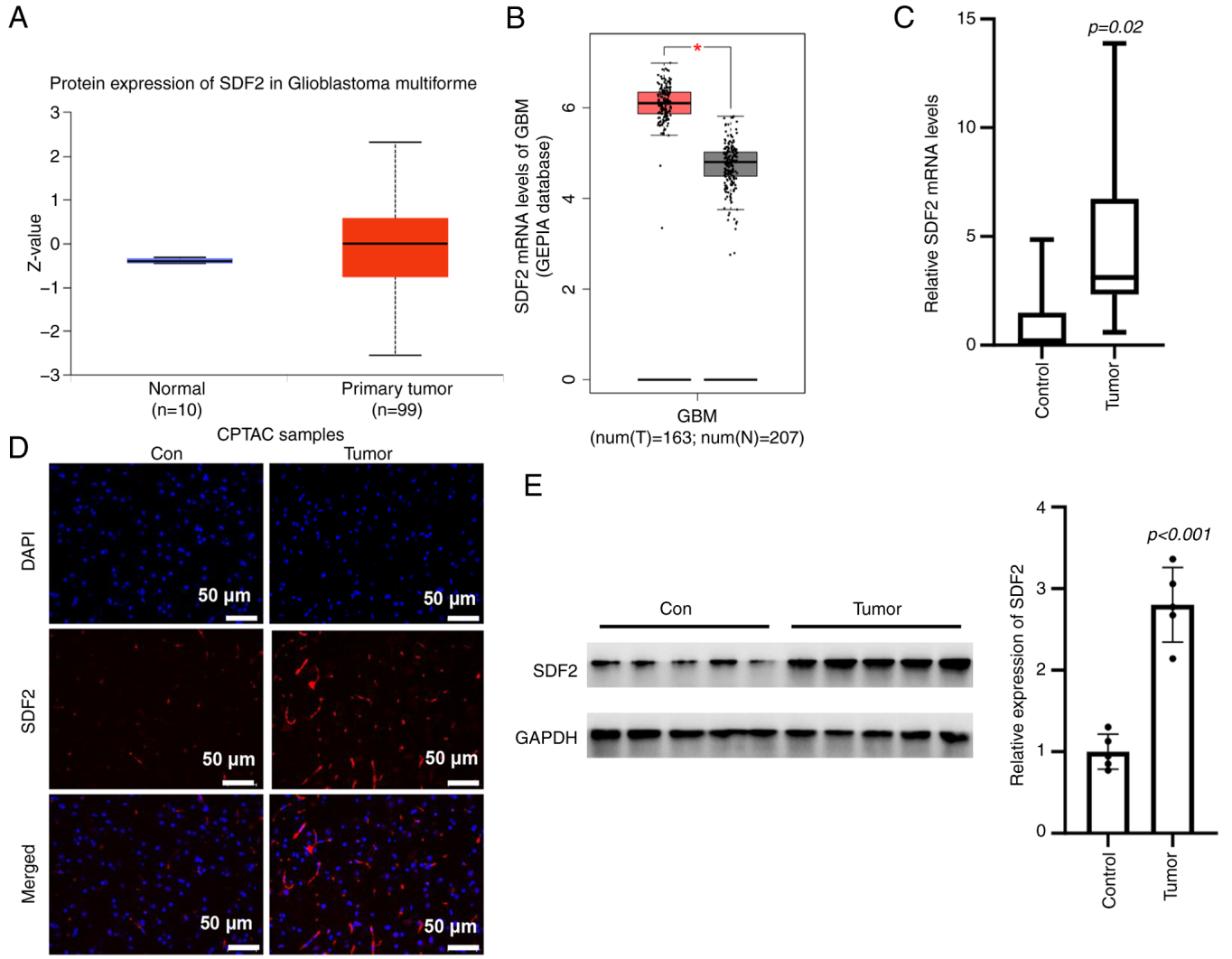

Figure 3. Expression of SDF2 is increased in glioma tissues. (A and B) Bioinformatic analysis of SDF2 mRNA levels in glioma tissues compared with those in control tissues using the GEPIA database. (C) The mRNA level of SDF2 was elevated in glioma tissues compared with adjacent normal tissues (n=10 for each group). (D) Immunofluorescent staining revealed that the intensity of SDF2 was increased in glioma and control tissues (n=3 for each group; scale bar, 50 μm). (E) Western blot analysis demonstrated that the protein levels of SDF2 were greater in glioma tissues than in adjacent nontumor tissues (n=5 for each group).

antioxidant capacity, and oxidative stress regulation in glioma cells.

SDF2 mediates the downregulation of ATP7A and ATP7B through the ERAD pathway. The effects of SDF2 on key proteins in the ER stress pathway were investigated. Compared with Ad-NC, Ad-shSDF2 increased GRP78 mRNA levels and the ratio of XBP1s/XBP1u in U87 and U251 cells, whereas CHOP mRNA levels remained unchanged (Fig. 7A and C). Additionally, Ad-shSDF2 increased GRP78 protein expression in both cell lines (Fig. 7B and D). To confirm the involvement of the proteasome degradation pathway in ATP7A and ATP7B downregulation, U87 and U251 cells were co-incubated with the proteasome inhibitor MG132. Compared with the control treatment, SDF2 knockdown reduced ATP7A and ATP7B expression, whereas MG132 treatment increased ATP7A and ATP7B expression (Fig. 7E-H). Notably, pretreatment with MG132 significantly reversed the Ad-shSDF2-induced reduction in ATP7A and ATP7B levels (Fig. 7E and F). Furthermore, compared with Ad-NC, Ad-shSDF2 increased DLAT aggregation within mitochondria; however, MG132 pretreatment reduced DLAT aggregation (Fig. 7G and H). These findings indicate that SDF2 knockdown promotes ATP7A and ATP7B degradation through a GRP78-mediated ER-associated degradation pathway, with potential downstream effects on mitochondrial DLAT accumulation.

SDF2 suppresses ATP7A and ATP7B expression via a GRP78-mediated mechanism. To investigate the role of GRP78 in this process, si-GRP78 was utilized to specifically knock down GRP78 expression. RT-qPCR analysis confirmed a significant reduction in GRP78 mRNA levels in U87 and U251 cells following si-GRP78 transfection (Fig. 8A and D). Western blot analysis further verified that si-GRP78 effectively suppressed GRP78 protein expression in both glioma cell lines (Fig. 8B and E). Importantly, GRP78 silencing also blocked the Ad-shSDF2-induced downregulation of ATP7A and ATP7B in U87 and U251 cells (Fig. 8B and E). Co-IP results demonstrated that knockdown of GRP78

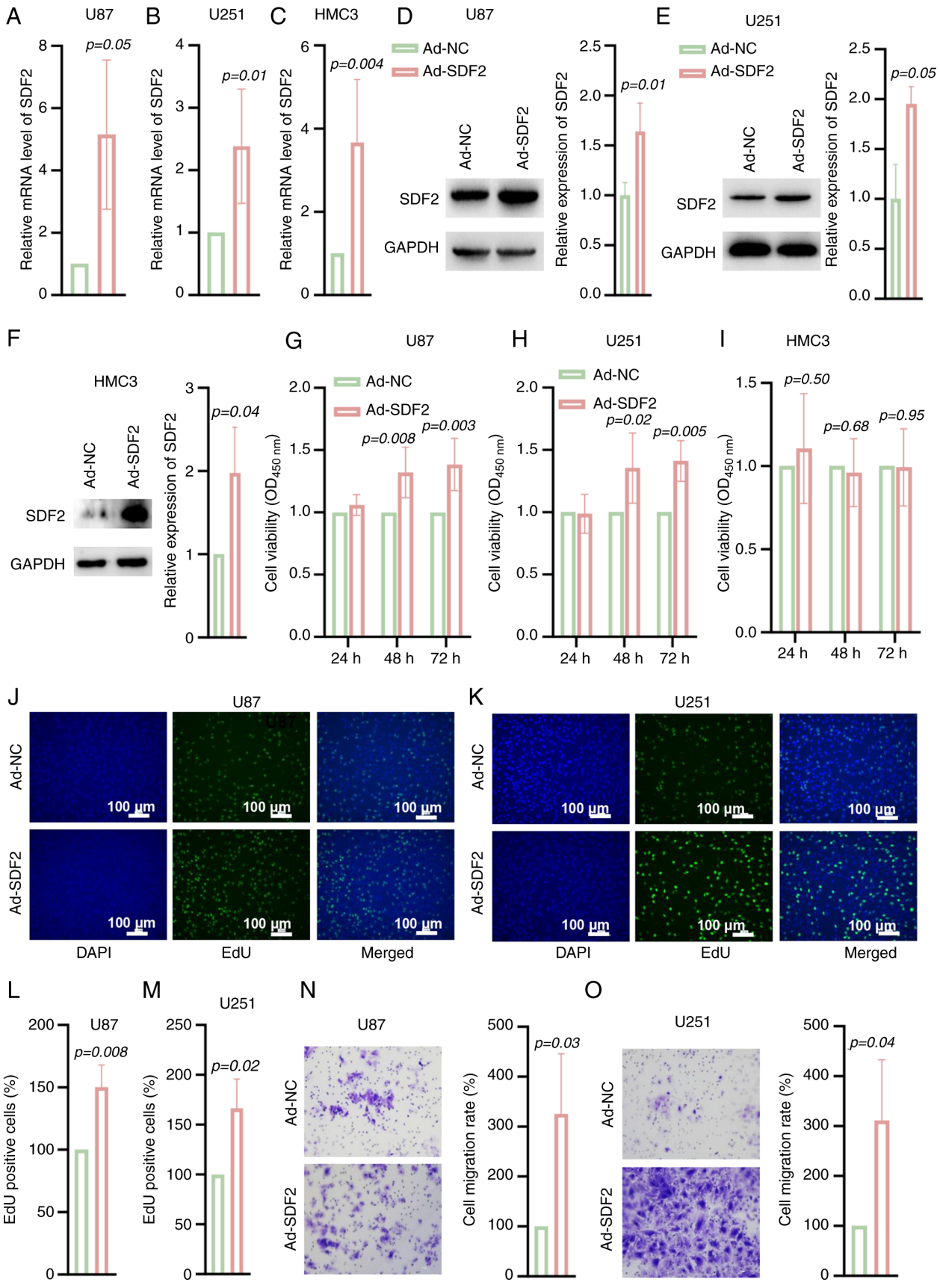

Figure 4. SDF2 promotes malignant proliferation and migration in glioma cells. (A-C) Reverse transcription-quantitative PCR analysis revealed that, compared with those in control cells, SDF2 mRNA levels were significantly elevated in U87, U251 and HMC3 cells following transfection with Ad-SDF2 (n=5). (D-F) SDF2 expression was upregulated in U87, U251 and HMC3 cells following transfection with Ad-SDF2 compared with that in control cells (n=3). (G-I) Cell viability assays demonstrated that SDF2 overexpression increased the viability of U87 and U251 cells in a time-dependent manner but did not affect the viability of HMC3 cells (n=5). (J-M) EdU staining revealed that the proliferative capacity of U87 and U251 cells was increased following SDF2 overexpression compared with that of control cells (n=3; scale bar, 100 μm). (N and O) Transwell migration assays revealed that the migratory ability of U87 and U251 cells overexpressing SDF2 was increased (n=3). SDF2, stromal cell-derived factor 2; NC, negative control.

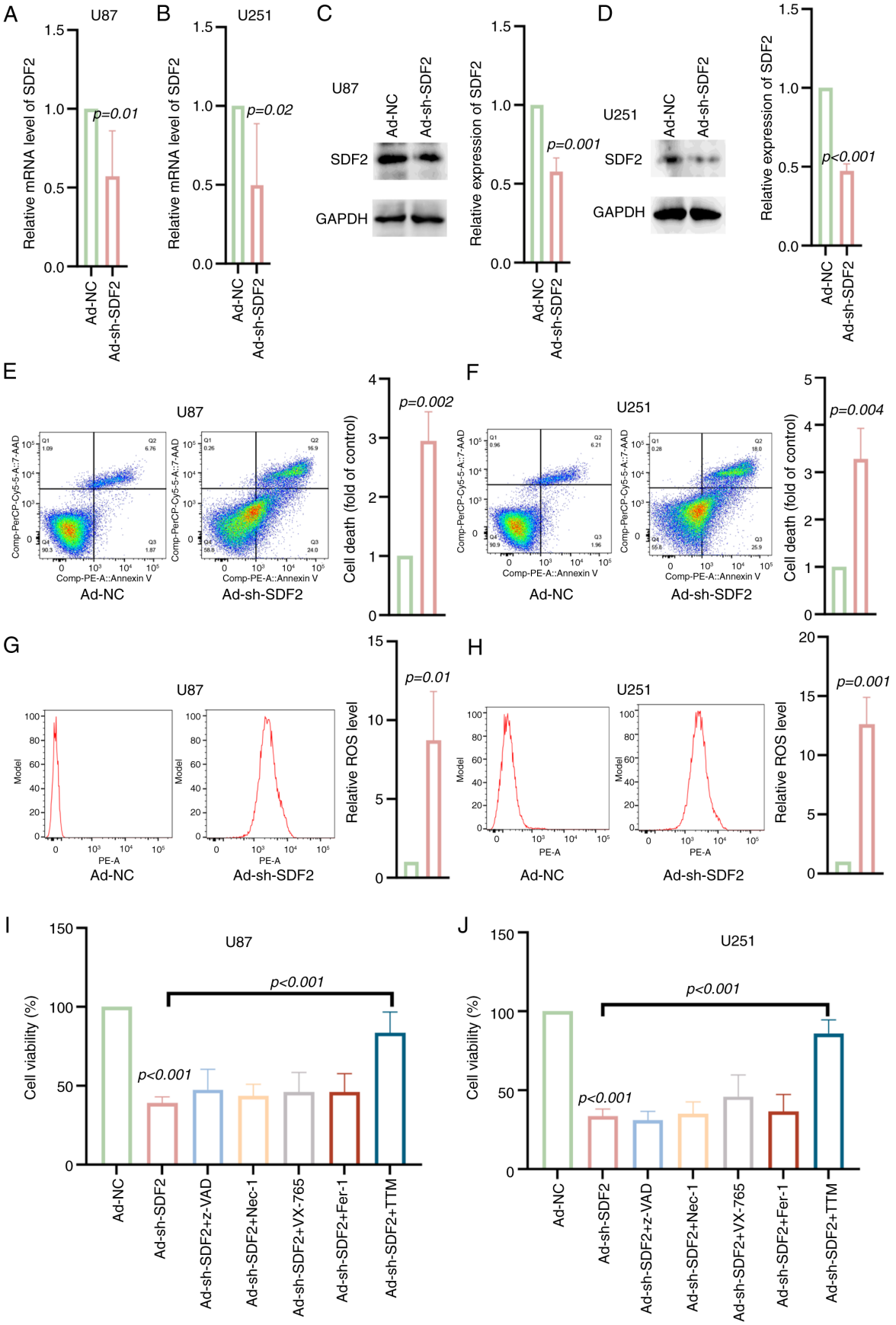

Figure 5. SDF2 knockdown increases ROS levels and apoptosis in glioma cells. (A and B) The mRNA levels of SDF2 were lower in U87 and U251 cells transfected with Ad-shSDF2 than in those transfected with Ad-NC (n=5). (C and D) Ad-shSDF2 decreased the expression of SDF2 in U87 and U251 cells (n=3). (E and F) Flow cytometric analysis revealed that the proportions of late apoptotic and necrotic cells were greater in U87 and U251 cells transfected with Ad-shSDF2 than in control cells (n=3). (G and H) Intracellular ROS levels were greater in U87 and U251 cells transfected with Ad-sh-SDF2 than in those transfected with Ad-NC (n=5). (I and J) Cell viability assays revealed that only the cuproptosis inhibitor TTM reversed the decrease in viability induced by Ad-shSDF2 in U87 and U251 cells (n=5). SDF2, stromal cell-derived factor 2; sh-, short hairpin; TTM, tetrathiomolybdate; NC, negative control.

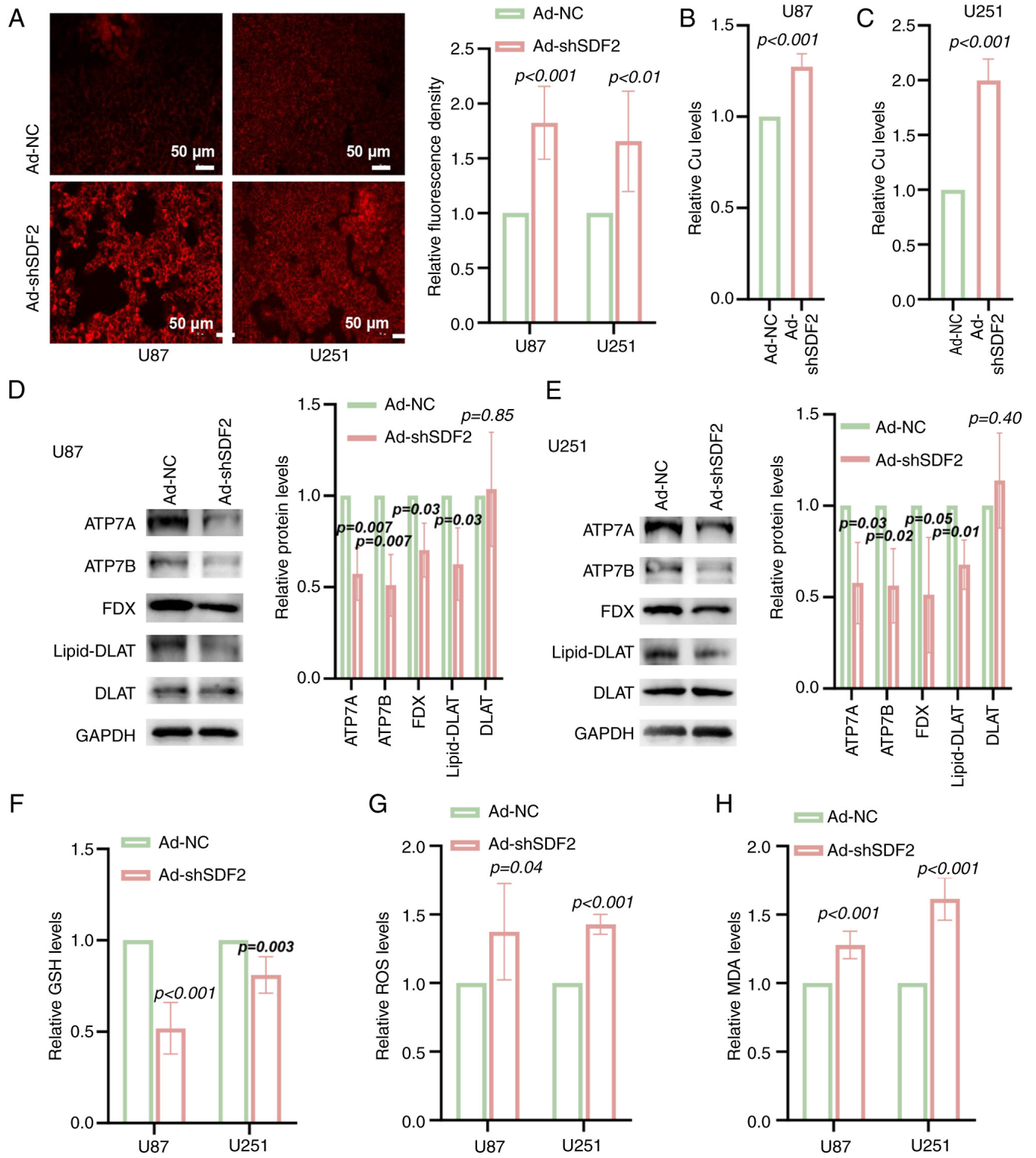

Figure 6. Knockdown of SDF2 increases intracellular copper ion accumulation and oxidative stress in glioma cells. (A) Fluorescence staining suggested that intracellular copper ion levels were elevated in U87 and U251 cells following SDF2 knockdown compared with those in control cells (n=3, scale bar, 50 μm). (B and C) Quantitative assessment of intracellular copper ion levels revealed significant copper accumulation in U87 and U251 cells upon SDF2 knockdown (n=5). (D and E) Western blot analysis revealed that ATP7A, ATP7B, FDX and lipid-DLAT expression was reduced, whereas DLAT protein expression did not significantly change (n=3). (F) A decrease in GSH was identified following SDF2 knockdown in U87 and U251 cells (n=5). (G and H) Increased ROS and MDA levels were detected in U87 and U251 cells upon SDF2 knockdown (n=3 for each group). SDF2, stromal cell-derived factor 2; DLAT, dihydrolipoamide S-acetyltransferase; GSH, reduced glutathione; ROS, reactive oxygen species; MDA, malondialdehyde; sh-, short hairpin; NC, negative control.

led to a reduction in the amount of ATP7A and ATP7B co-precipitated with GRP78. This decrease was observed after normalizing the Co-IP signals to GAPDH levels in the corresponding Input samples (Fig. 8C and F). These findings suggest that GRP78 may play a role in regulating ATP7A and ATP7B stability in glioma cells. Additionally,

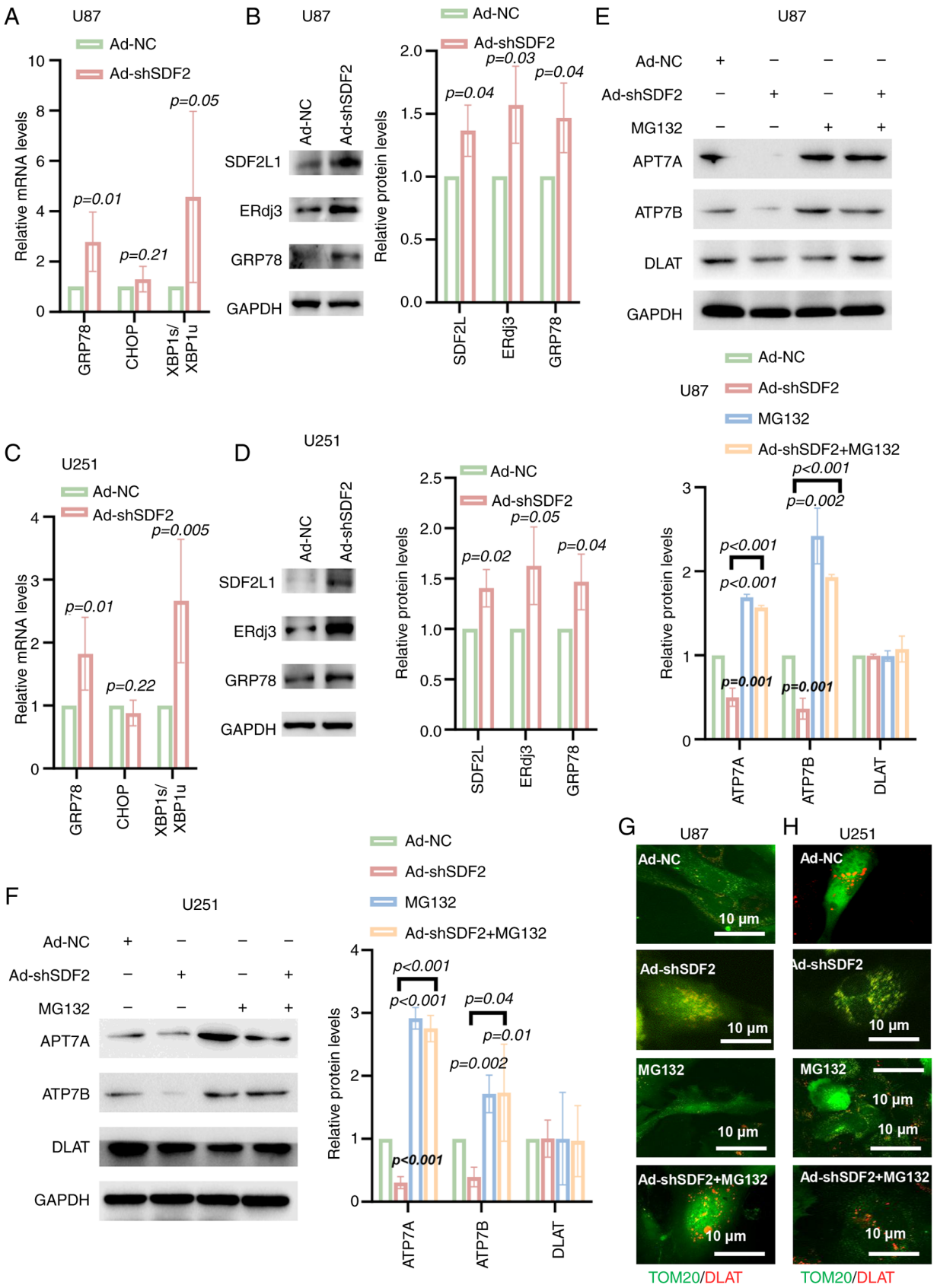

Figure 7. SDF2 knockdown mediates the downregulation of ATP7A and ATP7B via the endoplasmic reticulum-associated degradation pathway. (A and C) Reverse transcription-quantitative PCR analysis revealed that GRP78 mRNA levels and the XBP1s/XBP1u ratio were increased in U87 and U251 cells following Ad-shSDF2 transfection (n=5). (B and D) Western blot analysis demonstrated that the protein expression of GRP78, SDF2L and ERdj3 was increased in U87 and U251 cells after SDF2 knockdown (n=3). (E and F) Western blot analysis revealed that in U87 and U251 cells, SDF2 knockdown reduced ATP7A and ATP7B expression compared with that in control cells, whereas pretreatment with MG132 significantly reversed the Ad-shSDF2-induced reduction in ATP7A and ATP7B levels (n=3). (G and H) Immunofluorescent analysis revealed that DLAT aggregation was increased following Ad-shSDF2 transfection in U87 and U251 cells (n=3; scale bar, 10 μm). SDF2, stromal cell-derived factor 2; GRP78, glucose-related protein 78; XBP1, X-box binding protein 1; sh-, short hairpin; DLAT, dihydrolipoamide S-acetyltransferase; ERdj3, endoplasmic reticulum DnaJ heat shock protein 3; NC, negative control.

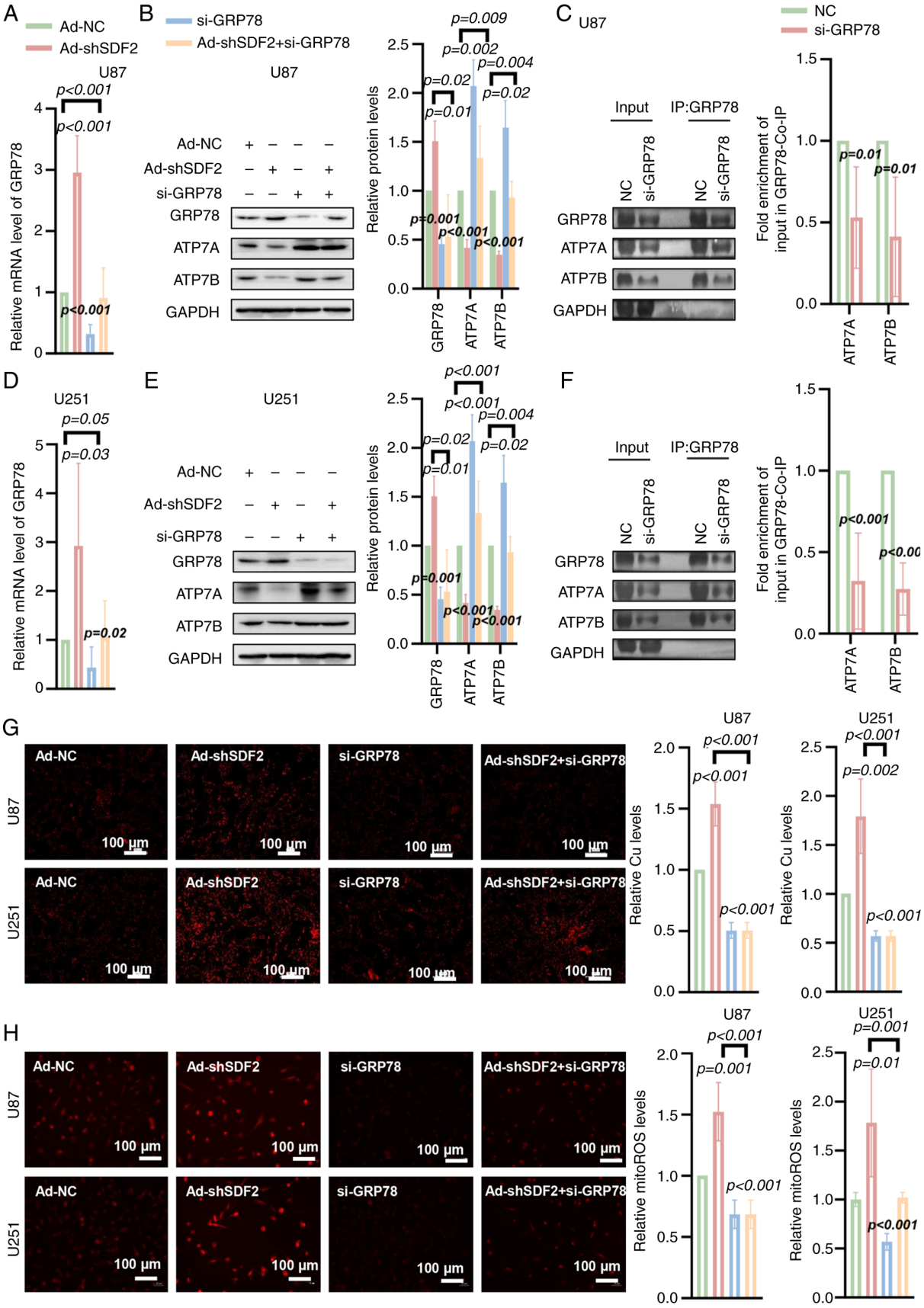

Figure 8. GRP78 mediates SDF2-induced downregulation of ATP7A and ATP7B in glioma cells. (A and D) Reverse transcription-quantitative PCR analysis showing that, compared with the control, transfection with si-GRP78 significantly reduced GRP78 mRNA levels in U87 and U251 cells (n=5). (B and E) Western blot analysis confirmed that GRP78 knockdown blocked the Ad-shSDF2-induced downregulation of ATP7A and ATP7B protein levels in both cell lines (n=3). (C and F) Co-immunoprecipitation analysis demonstrated that the association between GRP78 and ATP7A/ATP7B was reduced upon GRP78 knockdown in U87 and U251 cells (n=3). (G and H) GRP78 knockdown partially reversed the increase in Cu^{2+} levels and mito-ROS induced by Ad-shSDF2 in U87 and U251 cells (n=3; scale bar, 100 μm). GRP78, glucose-related protein 78; SDF2, stromal cell-derived factor 2; si-, small interfering; sh-, short hairpin; NC, negative control.

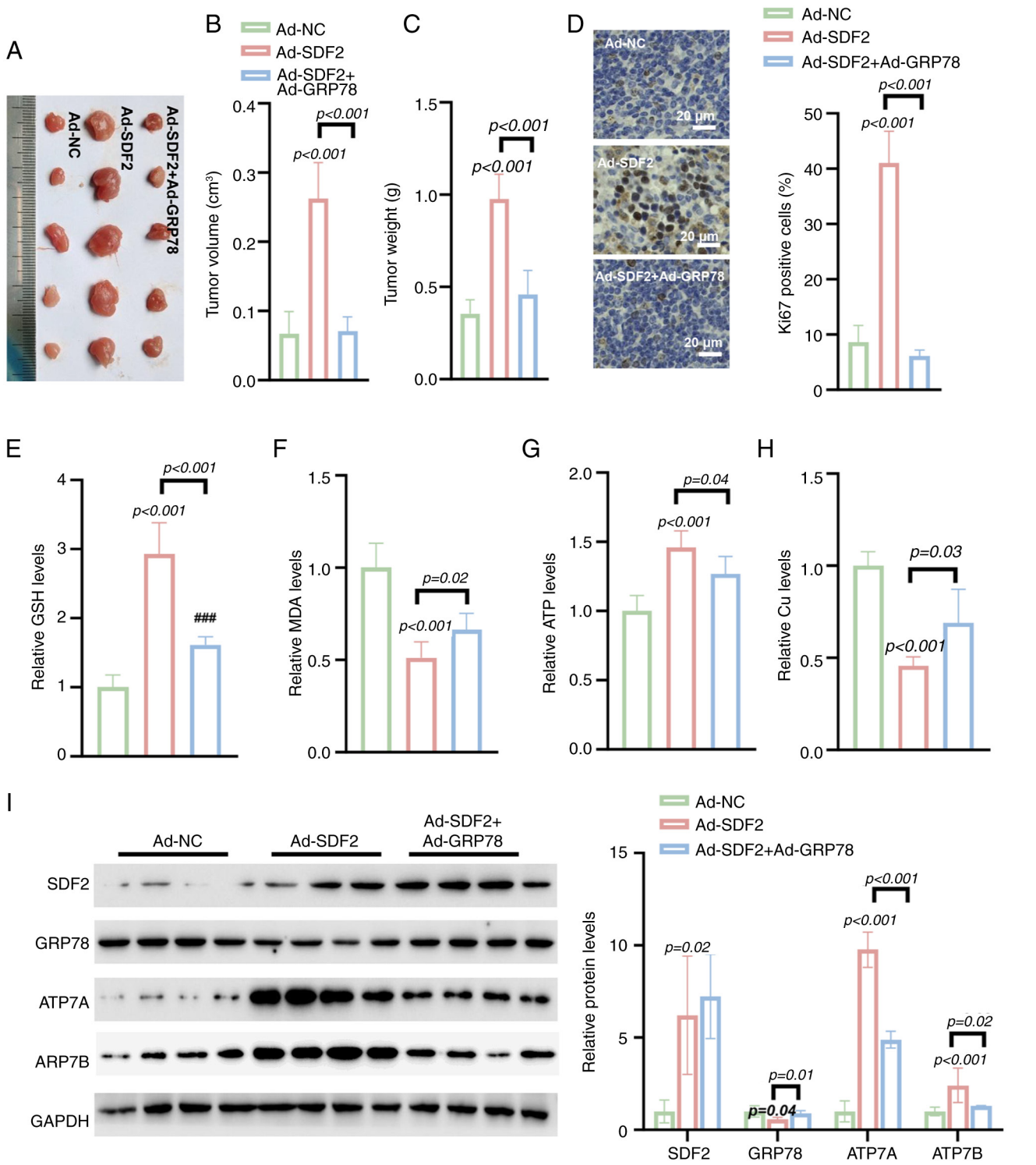

Figure 9. Ad-GRP78 reverses Ad-SDF2-induced tumor growth and metabolic changes in a nude mouse model. (A-C) Tumor size, volume and weight in nude mice injected with Ad-SDF2 or Ad-NC (n=5). (D) Immunohistochemical staining demonstrated that Ad-GRP78 co-expression reversed the Ad-SDF2-induced increase in Ki-67 positivity (n=5; scale bar, 20 μm). (E) Ad-SDF2 increased GSH levels, whereas Ad-GRP78 restored GSH levels in tumor tissues (n=5). (F) Ad-SDF2 reduced MDA levels, while Ad-GRP78 partially restored them (n=5). (G and H) Ad-SDF2 increased ATP and decreased Cu^{2+} levels, which were restored by Ad-GRP78 co-expression (n=5). (I) Western blot analysis showing that co-expressing Ad-GRP78 counteracted the Ad-SDF2-induced increases in ATP7A and ATP7B levels in tumor tissues (n=5). GRP78, glucose-related protein 78; SDF2, stromal cell-derived factor 2; GSH, reduced glutathione; MDA, malondialdehyde; NC, negative control.

GRP78 silencing partially reversed the Ad-shSDF2-induced increase in the intracellular Cu^{2+} and mito-ROS levels in U87 and U251 cells (Fig. 8G and H). These findings indicate that SDF2 suppresses ATP7A and ATP7B expression through a GRP78-dependent mechanism, impacting copper ion homeostasis and mitochondrial oxidative stress in glioma cells.

Ad-GRP78 reverses Ad-SDF2-induced tumor growth in vivo. Compared with Ad-NC, Ad-SDF2 significantly

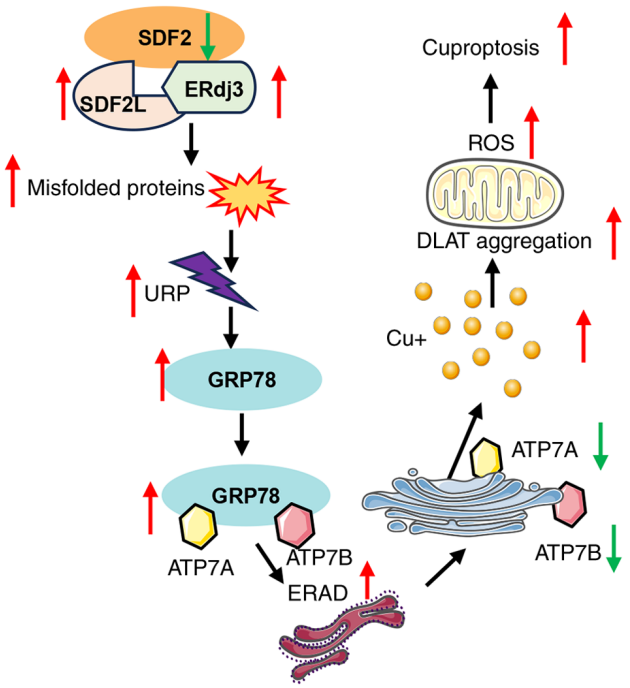

Figure 10. Schematic representation of the mechanism by which SDF2 contributes to glioma development. SDF2, stromal cell-derived factor 2; GRP78, glucose-related protein 78; DLAT, dihydrolipoamide S-acetyltransferase; ERdj3, endoplasmic reticulum DnaJ heat shock protein 3; ERAD, endoplasmic reticulum-associated degradation; ROS, reactive oxygen species; URP, unfolded protein response.

increased tumor volume, and weight in a nude mouse model (Fig. 9A-C). IHC analysis revealed that Ad-SDF2 increased the Ki-67 positivity rate in tumors, whereas the co-expression of Ad-GRP78 reversed this increase, suggesting an impact on cell proliferation (Fig. 9D). Further analysis revealed that Ad-SDF2 increased the GSH level in tumor tissues, which was effectively reversed by Ad-GRP78 (Fig. 9E). Similarly, Ad-SDF2 overexpression led to decreased MDA levels, whereas co-expression of Ad-GRP78 partially restored MDA levels (Fig. 9F). Moreover, Ad-SDF2 increased ATP levels and reduced Cu^{2+} concentrations in tumor tissues, while co-expression with Ad-GRP78 restored both parameters (Fig. 9G and H). Additionally, Ad-SDF2 overexpression suppressed GRP78 expression while increasing the expression of copper transporters ATP7A and ATP7B. Co-expression of Ad-GRP78 significantly reversed these changes (Fig. 9I). These findings indicate that GRP78 overexpression can counteract the effects of SDF2-induced changes in tumor growth and metabolism, highlighting the regulatory role of GRP78 in modulating SDF2-mediated changes in glioma growth and oxidative stress.

Discussion

Previous studies have shown that the expression of SDF2 is closely related to the development of breast and gastric cancers, highlighting its importance in tumor biology (20,21). Additionally, changes in SDF2 expression are associated with the occurrence of gestational diabetes and preeclampsia, further enhancing its potential as a biomarker (13). However, research on the role of SDF2 in glioma remains limited. The present study is the first to confirm the elevated expression of SDF2 in glioma samples. *In vitro* experiments demonstrated that SDF2 promotes the malignant proliferation and migration of glioma cells. These findings suggest that SDF2 may play a crucial role in the pathogenesis and progression of glioma. Further investigations are warranted to elucidate the underlying molecular mechanisms and explore the potential clinical applications of targeting SDF2 in glioma therapy.

In the present study, it was observed that the knockdown of SDF2 significantly increased the levels of ROS and enhanced the death of glioma cells. Transfection of U87 and U251 cells with Ad-shSDF2 resulted in a notable increase in the proportion of late apoptotic and necrotic cells, indicating that SDF2 depletion leads to increased cellular stress and compromised cell viability. Further analysis revealed that ROS levels were markedly elevated following SDF2 knockdown, suggesting a state of heightened oxidative stress. This finding is consistent with previous findings that link ROS accumulation to tumor progression and cell death in various cancer types, where oxidative stress has been shown to promote apoptotic pathways and influence tumor behavior (22,23). Interestingly, when the mechanisms underlying the observed decrease in cell viability were assessed, only the cuproptosis inhibitor TTM effectively reversed the effects of Ad-shSDF2. This finding highlights the specific involvement of copper-dependent cell death pathways in glioma cells, aligning with recent studies that highlight cuproptosis as a novel form of regulated cell death distinct from apoptosis and other forms of cell death, such as autophagy and ferroptosis (24,25). The selective reversal of cell viability impairment by the cuproptosis inhibitor suggested that SDF2 may play a role in modulating copper metabolism and its downstream effects on glioma cell survival.

SDF2-L1 is a close homologue of SDF2, thus, the expression of SDF2-L1 was detected in SDF2 knockdown cells. The present data showed that knockdown of SDF2 elevated the expression of SDF2-L1. These data indicated that SDF2-L1 may compensate the deficiency of SDF2. ERdj3, an abundant and soluble ER co-chaperone within the regulatory network of the Hsp70 family member BiP, stimulates BiP's ATPase activity to enhance its affinity for substrate proteins (26). Our findings confirmed that knockdown of SDF2 upregulated ERdj3 expression. It was hypothesized that SDF2 knockdown leads to dissociation of the SDF2-ERdj3 complex, resulting in accumulation of unfolded proteins, which triggers ER stress and subsequently induces the upregulation of both ERdj3 and GRP78 expression. Under homeostatic conditions, the SDF2-ERdj3 complex maintains ER homeostasis by suppressing the aggregation of unfolded proteins, thereby restraining the activation of UPR signaling pathways such as PERK and IRE1 (15). It is proposed that knockdown of SDF2 disrupts this complex, leading to the accumulation of unfolded proteins, which triggers ER stress and subsequently activates the UPR. This activation drives the transcriptional upregulation of GRP78 (27,28). In the present study, it was found that knockdown of SDF2 elevated XBPs/XBPu, indicating the activation of unfolded protein response (URP). Following activation of URP in glioma cells, the expression of GRP78 was

increased. As a multifunctional chaperone, GRP78 recruits core ERAD components (for example, Sec61, Derlin-1 and ubiquitin ligases) under stress conditions to retro-translocate misfolded protein to the cytoplasm for proteasomal degradation (29). Notably, GRP78 may facilitate the maturation of ATP7A/7B through its chaperone activity under non-stressed conditions but shifts toward a pro-degradative role during persistent ER stress. In the present study, it was observed that SDF2 knockdown in glioma cells led to increased levels of spliced XBP1, indicating activation of the UPR, which in turn upregulated GRP78 expression. This upregulation may shift GRP78's role from promoting the maturation of ATP7A and ATP7B to facilitating their degradation via ERAD, thereby impacting their expression levels.

The expression of FDX and Lipid-DLAT was also detected. The current data showed that the expression of FDX and Lipid-DLAT was reduced in U251 and U87 cells transfected with Ad-sh-SDF2 compared with that of Ad-NC. These data strengthened the cuproptosis link. In the process of cuproptosis, the aggregation of DLAT is a key feature. Studies have shown that during cuproptosis, DLAT aggregation results from the binding of copper ions to its lipoylated sites, forming insoluble aggregates, while the levels of DLAT are not changed (30-32). In the present study, it was observed that although DLAT aggregation increased in the Ad-SDF2 group, the total protein expression level of DLAT did not change significantly. This phenomenon may be due to the binding of copper ions to lipoylated DLAT, inducing the formation of high-molecular-weight aggregates, leading to loss of protein function, but these aggregates are not necessarily rapidly degraded, thus maintaining the total protein level unchanged. This suggests that DLAT aggregation is not due to protein degradation pathways reducing its expression level.

The *in vivo* experiments demonstrated that SDF2 overexpression led to increased tumor size, volume and weight in a nude mouse model, suggesting a significant role in promoting tumor proliferation, as indicated by increased Ki-67 positivity. This effect, however, was counteracted by co-expressing Ad-GRP78, which reversed the SDF2-induced increase in tumor growth and proliferation. These findings suggest that GRP78 plays a key regulatory role in modulating SDF2-mediated effects on glioma progression. GRP78, a well-established ER chaperone protein, facilitates protein folding and guides misfolded proteins to the ERAD pathway for subsequent degradation (33). In the context of cellular stress, GRP78 binds to misfolded proteins and initiates their transport to the ERAD system, where they are ubiquitinated and targeted for proteasomal degradation (34). In the present study, SDF2 overexpression downregulated GRP78, suggesting that reduced GRP78 expression impairs its ability to guide ATP7A and ATP7B to the ERAD pathway. Consequently, this leads to decreased degradation of these copper transport proteins, resulting in their increased expression (Fig. 10).

However, it is accepted that ATP7A and ATP7B are key copper-exporting transporters, and their downregulation may lead to intracellular copper accumulation, thereby triggering cuproptosis. The importance of rescue experiments was also acknowledged to validate this mechanism. While such experiments were not included in the current study, the authors plan to perform overexpression of ATP7A/B in future studies to further investigate their role in copper accumulation and cell death.

In summary, these findings collectively indicate that GRP78 overexpression counters SDF2-driven tumor growth and oxidative stress by enhancing the degradation of ATP7A and ATP7B through the ERAD pathway. These findings highlight the potential therapeutic value of modulating GRP78 to control SDF2-mediated effects in glioma, suggesting a novel approach to mitigate tumor growth and associated metabolic disruptions.

Acknowledgements

Not applicable.

Funding

The present study was supported by the Shaanxi Key Research and Development Plan Project (grant no. 2024SF-YBXM-215).

Availability of data and materials

The data generated in the present study may be requested from the corresponding author.

Authors' contributions

TW and JS designed the experiments and revised the manuscript. AL and XL performed the experiments. AL analyzed the data and wrote the manuscript. TW and JS confirmed the authenticity of all the raw data. All authors read and approved the final version of the manuscript.

Ethics approval and consent to participate

Human tumor and adjacent nontumor tissue samples were obtained from patients during surgical procedures, with informed consent obtained from all participants. Ethical approval for the collection and use of human samples was granted by the Institutional Review Board of the First Affiliated Hospital of Xi'an Jiaotong University (approval no. 2024SF-FAHX-212; Xi'an, China), in accordance with the ethical principles outlined in the Declaration of Helsinki. All animal experiments were conducted in compliance with institutional, national, and international guidelines, specifically adhering to the revised Animals (Scientific Procedures) Act 1986 (UK) and Directive 2010/63/EU (Europe). Approval for all animal experiments was granted by the Institutional Ethics Committee of the Animal Experimentation Center, Xi'an Jiaotong University (approval no. XJTUAE2023-1944; Xi'an, China).

Patient consent for publication

Not applicable.

Competing interests

The authors declare that they have no competing interests.

References

1. Wang LM, Englander ZK, Miller ML and Bruce JN: Malignant glioma. Adv Exp Med Biol 1405: 1-30, 2023.
2. Weller M, Wen PY, Chang SM, Dirven L, Lim M, Monje M and Reifenberger G: Glioma. Nat Rev Dis Primers 10: 33, 2024.
3. Hakar MH and Wood MD: Updates in pediatric glioma pathology. Surg Pathol Clin 13: 801-816, 2020.
4. Wei R, Zhou J, Bui B and Liu X: Glioma actively orchestrate a self-advantageous extracellular matrix to promote recurrence and progression. BMC Cancer 24: 974, 2024.
5. Krshnan L, van de Weijer ML and Carvalho P: Endoplasmic reticulum-associated protein degradation. Cold Spring Harb Perspect Biol 14: a041247, 2022.
6. Zhou Z, Torres M, Sha H, Halbrook CJ, Van den Bergh F, Reinert RB, Yamada T, Wang S, Luo Y, Hunter AH, *et al*: Endoplasmic reticulum-associated degradation regulates mitochondrial dynamics in brown adipocytes. Science 368: 54-60, 2020.
7. Turk SM, Indovina CJ, Miller JM, Overton DL, Runnebohm AM, Orchard CJ, Tragesser-Tiña ME, Gosser SK, Doss EM, Richards KA, *et al*: Lipid biosynthesis perturbation impairs endoplasmic reticulum-associated degradation. J Biol Chem 299: 104939, 2023.
8. Stevenson J, Huang EY and Olzmann JA: Endoplasmic reticulum-associated degradation and lipid homeostasis. Annu Rev Nutr 36: 511-542, 2016.
9. Xu Y and Fang D: Endoplasmic reticulum-associated degradation and beyond: The multitasking roles for HRD1 in immune regulation and autoimmunity. J Autoimmun 109: 102423, 2020.
10. Sun S, Shi G, Sha H, Ji Y, Han X, Shu X, Ma H, Inoue T, Gao B, Kim H, *et al*: IRE1α is an endogenous substrate of endoplasmic-reticulum-associated degradation. Nat Cell Biol 17: 1546-1555, 2015.
11. Zhang MJ, Shi M, Yu Y, Ou R, Ge RS and Duan P: Curcuminoid PBPD induces cuproptosis and endoplasmic reticulum stress in cervical cancer via the Notch1/RBP-J/NRF2/FDX1 pathway. Mol Carcinog 63: 1449-1466, 2024.
12. Gu Y, Wang H, Xue W, Zhu L, Fu C, Zhang W, Mu G, Xia Y, Wei K and Wang J: Endoplasmic reticulum stress related super-enhancers suppress cuproptosis via glycolysis reprogramming in lung adenocarcinoma. Cell Death Dis 16: 316, 2025.
13. Lorenzon-Ojea AR, Yung HW, Burton GJ and Bevilacqua E: The potential contribution of stromal cell-derived factor 2 (SDF2) in endoplasmic reticulum stress response in severe preeclampsia and labor-onset. Biochim Biophys Acta Mol Basis Dis 1866: 165386, 2020.
14. Hanafusa K, Wada I and Hosokawa N: SDF2-like protein 1 (SDF2L1) regulates the endoplasmic reticulum localization and chaperone activity of ERdj3 protein. J Biol Chem 294: 19335-19348, 2019.
15. Fujimori T, Suno R, Iemura SI, Natsume T, Wada I and Hosokawa N: Endoplasmic reticulum proteins SDF2 and SDF2L1 act as components of the BiP chaperone cycle to prevent protein aggregation. Genes Cells 22: 684-698, 2017.
16. Livak KJ and Schmittgen TD: Analysis of relative gene expression data using real-time quantitative PCR and the 2(-Delta Delta C(T)) Method. Methods 25: 402-408, 2001.
17. DiVita Dean B, Wildes T, Dean J, Yegorov O, Yang C, Shin D, Francis C, Figg JW, Sebastian M, Font LF, *et al*: Immunotherapy reverses glioma-driven dysfunction of immune system homeostasis. J Immunother Cancer 11: e004805, 2023.
18. Zhang Y, Xiang Z, Chen L, Deng X, Liu H and Peng X: PSMA2 promotes glioma proliferation and migration via EMT. Pathol Res Pract 256: 155278, 2024.
19. Zamler DB, Shingu T, Kahn LM, Huntoon K, Kassab C, Ott M, Tomczak K, Liu J, Li Y, Lai I, *et al*: Immune landscape of a genetically engineered murine model of glioma compared with human glioma. JCI Insight 7: e148990, 2022.
20. Gong W, Martin TA, Sanders AJ, Jiang A, Sun P and Jiang WG: Location, function and role of stromal cell-derived factors and possible implications in cancer (Review). Int J Mol Med 47: 435-443, 2021.
21. Wang Y, Zheng M, Du S, Wang P, Zhang T, Zhang X and Zu G: Clinicopathological and prognostic significance of stromal cell derived factor 2 in the patients with gastric cancer. BMC Gastroenterol 24: 325, 2024.
22. Slika H, Mansour H, Wehbe N, Nasser SA, Iratni R, Nasrallah G, Shaito A, Ghaddar T, Kobeissy F and Eid AH: Therapeutic potential of flavonoids in cancer: ROS-mediated mechanisms. Biomed Pharmacother 146: 112442, 2022.
23. Jelic MD, Mandic AD, Maricic SM and Srdjenovic BU: Oxidative stress and its role in cancer. J Cancer Res Ther 17: 22-28, 2021.
24. Wang J, Li S, Guo Y, Zhao C, Chen Y, Ning W, Yang J and Zhang H: Cuproptosis-related gene SLC31A1 expression correlates with the prognosis and tumor immune microenvironment in glioma. Funct Integr Genomics 23: 279, 2023.
25. Zhang B, Xie L, Liu J, Liu A and He M: Construction and validation of a cuproptosis-related prognostic model for glioblastoma. Front Immunol 14: 1082974, 2023.
26. Guo F and Snapp EL: ERdj3 regulates BiP occupancy in living cells. J Cell Sci 126: 1429-1439, 2013.
27. Lorenzon-Ojea AR, Guzzo CR, Kapidzic M, Fisher SJ and Bevilacqua E: Stromal cell-derived factor 2: A novel protein that interferes in endoplasmic reticulum stress pathway in human placental cells. Biol Reprod 95: 41, 2016.
28. Ibrahim IM, Abdelmalek DH and Elfiky AA: GRP78: A cell's response to stress. Life Sci 226: 156-163, 2019.
29. Cesaratto F, Sasset L, Myers MP, Re A, Petris G and Burrone OR: BiP/GRP78 mediates ERAD targeting of proteins produced by membrane-bound ribosomes stalled at the STOP-Codon. J Mol Biol 431: 123-141, 2019.
30. Hu F, Huang J, Bing T, Mou W, Li D, Zhang H, Chen Y, Jin Q, Yu Y and Yang Z: Stimulus-responsive copper complex nanoparticles induce cuproptosis for augmented cancer immunotherapy. Adv Sci (Weinh) 11: e2309388, 2024.
31. Qi RQ, Chen YF, Cheng J, Song JW, Chen YH, Wang SY, Liu Y, Yan KX, Liu XY, Li J and Zhong JC: Elabela alleviates cuproptosis and vascular calcification in vitaminD3- overloaded mice via regulation of the PPAR-γ /FDX1 signaling. Mol Med 30: 223, 2024.
32. Xiao Y, Yin J, Liu P, Zhang X, Lin Y and Guo J: Triptolide-induced cuproptosis is a novel antitumor strategy for the treatment of cervical cancer. Cell Mol Biol Lett 29: 113, 2024.
33. Cai X, Ito S, Noi K, Inoue M, Ushioda R, Kato Y, Nagata K and Inaba K: Mechanistic characterization of disulfide bond reduction of an ERAD substrate mediated by cooperation between ERdj5 and BiP. J Biol Chem 299: 105274, 2023.
34. Akinyemi AO, Simpson KE, Oyelere SF, Nur M, Ngule CM, Owoyemi BCD, Ayarick VA, Oyelami FF, Obaleye O, Esoe DP, *et al*: Unveiling the dark side of glucose-regulated protein 78 (GRP78) in cancers and other human pathology: A systematic review. Mol Med 29: 112, 2023.